











High fusion performance in Super H-mode experiments on Alcator C-Mod and DIII-D

P.B. Snyder¹, J.W. Hughes², T.H. Osborne¹, C. Paz-Soldan¹,
W.M. Solomon¹, M. Knolker³, D. Eldon¹, T. Evans¹, T. Golfopoulos²,
B.A. Grierson³, R.J. Groebner¹, A.E. Hubbard², E. Kolemen³,
B. LaBombard², F.M. Laggner³, O. Meneghini¹, S. Mordijck⁴, T. Petrie¹,
S. Scott³, H.Q. Wang¹, H.R. Wilson^{5,6} and Y.B. Zhu⁷

¹ General Atomics, San Diego, CA, United States of America

² MIT Plasma Science and Fusion Center, Cambridge, MA, United States of America

³ Princeton Plasma Physics Laboratory, Princeton University, Princeton, NJ, United States of America

⁴ College of William and Mary, Williamsburg, VA, United States of America

⁵ York Plasma Institute, University of York, York, United Kingdom of Great Britain and Northern Ireland

⁶ Culham Center for Fusion Energy, Culham Science Centre, Abingdon, Oxon, United Kingdom of Great Britain and Northern Ireland

⁷ University of California Irvine, Irvine, CA, United States of America

E-mail: snyder@fusion.gat.com

Received 10 January 2019, revised 2 May 2019

Accepted for publication 21 May 2019

Published 24 June 2019



CrossMark

Abstract

The ‘Super H-Mode’ regime is predicted to enable pedestal height and fusion performance substantially higher than standard H-Mode operation. This regime exists due to a bifurcation of the pedestal pressure, as a function of density, that is predicted by the EPED model to occur in strongly shaped plasmas above a critical pedestal density. Experiments on Alcator C-Mod and DIII-D have achieved access to the Super H-Mode (and Near Super H) regime, and obtained very high pedestal pressure, including the highest achieved on a tokamak ($p_{\text{ped}} \sim 80$ kPa) in C-Mod experiments operating near the ITER magnetic field. DIII-D Super H experiments have demonstrated strong performance, including the highest stored energy in the present configuration of DIII-D ($W \sim 2.2\text{--}3.2$ MJ), while utilizing only about half of the available heating power ($P_{\text{heat}} \sim 7\text{--}12$ MW). These DIII-D experiments have obtained the highest value of peak fusion gain, $Q_{\text{DT,equiv}} \sim 0.5$, achieved on a medium scale ($R < 2$ m) tokamak. Sustained high performance operation ($\beta_{\text{N}} \sim 2.9$, $H_{98} \sim 1.6$) has been achieved utilizing $n = 3$ magnetic perturbations for density and impurity control. Pedestal and global confinement has been maintained in the presence of deuterium and nitrogen gas puffing, which enables a more radiative divertor condition. A pair of simple performance metrics is developed to assess and compare regimes. Super H-Mode access is predicted for ITER and expected, based on both theoretical prediction and observed normalized performance, to allow ITER to achieve its goals ($Q = 10$) at $I_{\text{p}} < 15$ MA, and to potentially enable more compact, cost effective pilot plant and reactor designs.

Keywords: pedestal, tokamak, fusion gain, Super H Mode, EPED, DIII-D, Alcator C-Mod

(Some figures may appear in colour only in the online journal)



1. Introduction—the EPED model and prediction of the Super H regime

In a tokamak, the edge transport barrier, or ‘pedestal,’ region plays a critical role in both fusion performance and compatibility with desired divertor conditions. The pressure at the top of the pedestal, or ‘pedestal height,’ strongly impacts global confinement and fusion performance, with fusion power production expected to scale approximately with the square of the pedestal height. The density at the interface between the pedestal and open field line region, i.e. the separatrix density, must be consistent with a divertor solution that enables low temperatures and minimal erosion at material surfaces.

The EPED model [1–4] is developed based on the hypothesis that, while many mechanisms drive transport across the edge barrier, evolution of the pressure profile in this region is typically constrained by the onset of nearly local kinetic ballooning modes (KBM) and non-local peeling–ballooning (P–B) modes driven by a combination of pressure and current gradients. EPED predicts the H-mode pedestal height and width in high performance regimes, including regimes with ‘Type I’ edge localized modes (ELMs) and regimes with a quiescent (‘QH Mode’) edge and edge harmonic oscillations (EHOs) [2], based upon criticality to these two constraints. These calculations are performed on realistic model equilibria, with self-consistent bootstrap current in the pedestal region, to enable pedestal predictions for future experiments and future devices. The combination of P–B and KBM physics leads to strong dependencies of the pedestal height on poloidal field (B_p), toroidal field (B_t) and plasma shape, which have been successfully tested in several experiments (e.g. [1–10]). An important dependence on pedestal density (which is an input to EPED) derives primarily from the variation of the bootstrap current with collisionality. In most circumstances, the EPED model predicts a single pedestal solution, at the intersection of P–B and KBM criticality (see figure 1(a)). However, for very strongly shaped plasmas (typically triangularity $\delta > \sim 0.45$, for $q_{95} \sim 3.5\text{--}5$, $R/a \sim 3$, elongation $\sim 1.7\text{--}2$), above a critical density, the solution can bifurcate into three solutions. In this circumstance we denote the lower pressure solution the ‘H-mode’ solution, and the two higher pressure solutions ‘Super H-mode’ (SH) solutions because they sit above the H-mode solution in pressure (at the same set of EPED input parameters, including density, Z_{eff} , shape, current, field, and major and minor radius). The SH solutions may initially appear to be of limited practical interest, because they sit above a P–B unstable region, and P–B modes are known to drive either ELMs or EHOs which prevent further increases in pressure. However, diagrams such as figure 1(a) are drawn for a fixed set of input parameters. By varying key parameters, for example by reducing the pedestal density, it is possible to shrink the P–B unstable region between the H and SH solutions until it disappears, leaving only a single (what was the highest pressure) solution. After the pedestal rises to this solution, the pedestal density can then be increased, leaving the discharge in SH. This sort of parametric trajectory can be visualized (magenta arrow) in figure 1(b), starting at high pedestal density (along black line at the right), decreasing the density

until only the blue solution remains, then increasing density to access the red SH solutions. Note that the blue ‘Near Super H’ (NSH) regime shown in figure 1(b) also results in higher pedestal pressure than for typical H-modes (black lines). Coupled core-pedestal modeling [11–14] predicts elevated fusion performance should be obtainable in both the NSH and SH regimes.

Accessing the Super H regime experimentally requires a strongly shaped plasma at moderate $q_{95} \sim 3.5\text{--}5$, and an appropriate parametric trajectory for the density. The Super H regime was first discovered experimentally on DIII-D, in a series of experiments guided by prior theoretical predictions [15, 16]. These initial experiments were conducted with neutral beam injection in the counter-current direction, and generally had a quiescent (QH mode) edge, which enabled a smooth increase of the density in the Super H regime. Additional DIII-D experiments and predictive modeling have explored the parameter regime for SH access on DIII-D, and the potential benefits for fusion performance [16–18].

In the following sections we describe more recent SH experiments on Alcator C-Mod and on DIII-D (experiments on C-Mod during its final month of operations in September 2016, and experiments on DIII-D, with co-current NBI and ELMs, from June 2017–April 2018). These experiments were aimed at further testing of EPED model predictions, as well as realization of very high pedestals, strong fusion performance, and investigation of dissipative divertor operation. In section 2, we describe experiments accessing the Super H regime with very high pedestal and global pressure on C-Mod, and large stored energy and fusion gain on DIII-D. In section 3, we describe progress toward sustainment of SH/NSH discharges on DIII-D, using 3D magnetic perturbations to drive density and impurity transport, and initial study of the compatibility of high core and pedestal performance with strong deuterium and nitrogen puffing in the divertor region.

2. Achieving Super H access and high peak performance

The high pedestal pressure and ion temperature predicted and observed in the SH and NSH regimes is expected to enable enhanced global pressure and confinement. This is due both to the nature of gradient-scale-length-driven turbulent transport in the core, which causes core temperature and pressure to rise with the pedestal, and to the broad pressure profiles enabled by a high pedestal, which have increased global MHD limits. Achieving this level of performance requires both successfully accessing the SH/NSH regime, and avoiding issues such as impurity accumulation and large-scale instabilities such as strong tearing modes in the core.

Following the prediction and observation of SH on DIII-D, predictions were undertaken for additional devices, including Alcator C-Mod and ITER. Predictions were made for Alcator C-Mod by starting with parameters from a high triangularity ($\delta = 0.49$) ELMing H-mode (1101214029), and varying the pedestal density over a wide range (figure 2(a)). These calculations indicate that the density required to access the

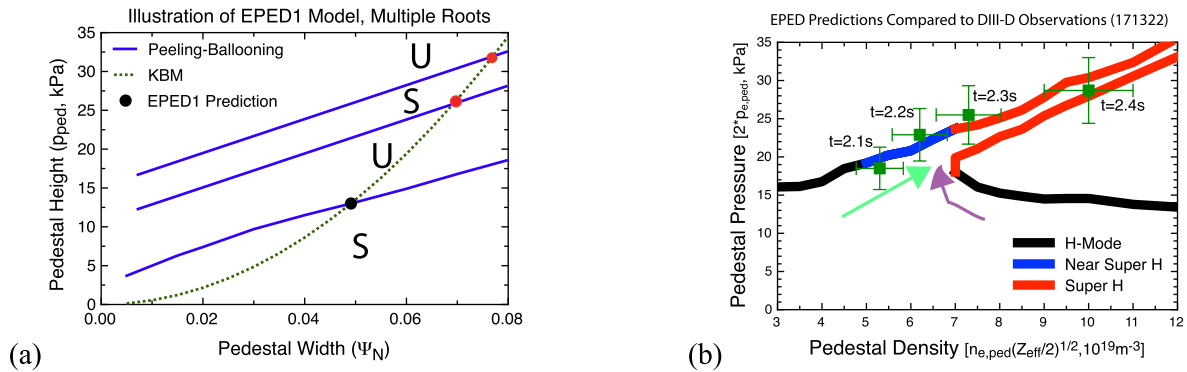


Figure 1. (a) Illustration of the EPED model, which predicts pedestal height and width via calculated P–B (blue lines) and KBM (green dashed line) constraints. Most commonly only a single solution (black circle) is found, but for strong shaping above a critical density, this solution bifurcates and two additional solutions (red circles), called ‘Super H mode’ (SH) solutions are found. (b) EPED predictions as a function of density indicate paths to SH (arrows) via reaching sufficiently low pedestal density, and then increasing density over time. The green squares are measurements from DIII-D discharge 171322 at 1.6 MA. Good agreement is found between the DIII-D observations and the EPED predictions (thick red, blue and black lines), which indicate access to the Near Super H and Super H regime.

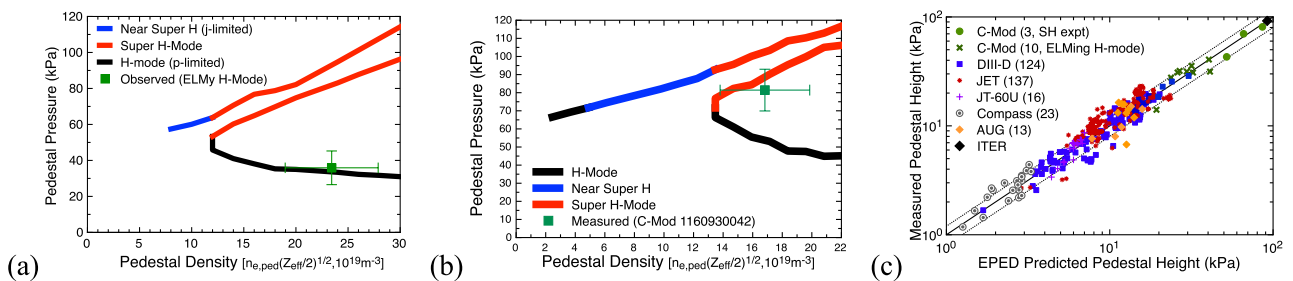


Figure 2. (a) EPED predictions (solid lines) based on a high triangularity $\delta = 0.49$, $I_p = 0.9$ MA, $B_t = 5.5$ T, Alcator C-Mod ELMy H-mode discharge indicate that the observed ELMy operational point (green square) is consistent with predictions for a pressure-limited H-mode pedestal (black line). The predictions also indicate potential access to SH (red lines) and NSH (blue line) by going to lower pedestal density. (b) EPED predictions for pedestal pressure versus density (solid lines) including the predicted region of Super-H (red lines) and Near Super H (blue line) access, compared to observations from C-Mod 1160930042 at $I_p = 1.4$ MA, $B_t = 5.8$ T. (c) EPED predicted pedestal height (p_{ped}) compared to observations on six devices, incorporating new results from C-Mod (green circles) Super H experiments. The prediction for ITER baseline is also shown (black diamond).

SH/NSH regime is substantially lower than typical operating densities on C-Mod (e.g. the green cross in figure 2(a)).

Accessing low normalized density in H-mode presents challenges, particularly in a high-Z metal wall device such as C-Mod, because (a) the L–H power threshold rises substantially below a particular density (on C-Mod, typically line average density below 10^{20} m^{-3}) [19, 20], (b) impurities can accumulate leading to large radiative losses before ELMs or other edge modes are driven strongly enough to regulate core impurity accumulation. A fortuitous discovery enabled successful access to the required low density regimes. By starting application of auxiliary ion cyclotron RF heating with the grad-B drift direction away from the active x -point (here upper single null), it is possible to first access the I-mode regime [21, 22], leading to a relatively low density, high temperature edge plasma. Then by transitioning the magnetic balance to direct the grad-B drift direction toward the x -point (here lower single null), the discharge can enter H-mode at low density and high temperature with low impurity content.

Employing this technique, C-Mod discharges at 0.8, 1.0, and 1.4 MA were able to access the NSH/SH region [23]. Pedestal densities as low as $7 \cdot 10^{19} \text{ m}^{-3}$ (among the lowest ever achieved on C-Mod) and $T_{ped} > 1.4 \text{ keV}$ were routinely

achieved. Discharges with intentionally lowered triangularity exhibited low- n ($n = 1$) edge modes, consistent with encountering the predicted current-driven kink/peeling mode limit (upper blue/red boundary in figures 2(a) and (b)). Starting at these low densities, the pedestal pressure increased with increasing density, consistent with expectation from theory, and pedestal pressures as high as 70 kPa at 1 MA, and 81 kPa at 1.4 MA were achieved. The $p_{ped} = 81$ kPa discharge (1160930042) has the highest pedestal pressure reported on any tokamak, and (figure 2(b)) is consistent with access to the Super H regime. The plasma cross section and density and temperature profiles for the highest pedestal pressure case (1160930042) are shown in figure 3(a). This 1.4 MA, 5.8 T case had a product of toroidal and poloidal field comparable ($\sim 90\%$) to the ITER values, and it achieved a pedestal pressure roughly 90% of the EPED predicted value for the ITER baseline. These discharges on C-Mod enabled comparisons of the EPED model with observations to extend across two orders of magnitude (a factor of 70 between the highest and lowest measured pedestal pressure) on six devices, up to values very close to the ITER prediction (figure 2(c), green circles are new data from C-Mod SH experiments). The agreement between the model and observations ($\sigma \sim 0.22$) is similar at low and

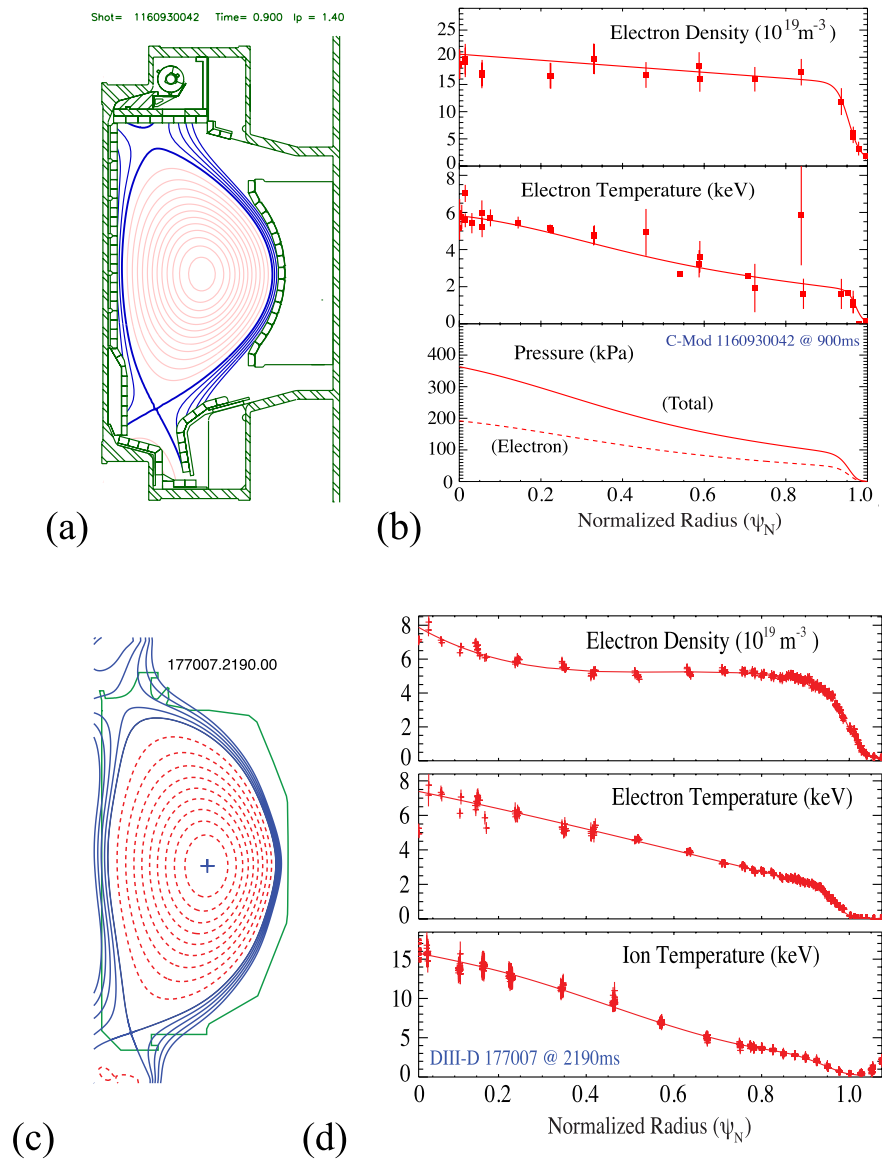


Figure 3. (a) Cross section and (b) measured density, electron temperature, and pressure profiles for Alcator C-Mod 1160930042, with $p_{\text{ped}} \sim 80$ kPa. (c) Cross section and (d) measured density and electron and ion temperature profiles for DIII-D 177007, $t = 2190$ ms, near the time of maximum stored energy ($W_{\text{MHD}} \sim 3.2$ MJ).

high pressure, with no indication of substantial variation in the level of agreement based on pressure or normalized gyro-radius (ρ^*) across the studied range.

On DIII-D, a series of experiments have been undertaken in co-injected discharges to explore SH and NSH access and sustainment across a wide range of plasma current ($I_p = 1.45$ – 2 MA) at full field ($B_t = 2.0$ – 2.2 T) and a range of high triangularity ($\delta \sim 0.5$ – 0.7). These discharges undergo an initial L-H transition at low density, and then the density increases over time to reach the SH/NSH regime (see figure 1(b)). Deuterium gas puffing, pumping, and active density control using 3D ($n = 3$) magnetic perturbations from the internal coil ('I-coil') are used to control pedestal density and impurity accumulation. Because these discharges use co-injection, that is injection of neutral beam power in the direction of the plasma current, (unlike most prior DIII-D Super H experiments which used counter-injection [16–18]), the edge exhibits edge

localized modes (ELMs), which in some cases onset during the density rise, and in other cases onset later after high pressure is obtained. These ELMs do not, by themselves, generally limit access to the Super H regime. The 1.6 MA case shown in figure 1(b) exhibited several ELMs during its rise, and the measurements (green squares) are taken shortly before these ELMs. Co-injection leads to more favorable current profiles in the core, enabling high values of peak ($\beta_N \sim 3.9$) and sustained ($\beta_N \sim 2.9$) beta, and also leads to significant co-rotation, which can enhance core confinement.

Experiments at higher current ($I_p = 1.8$ – 1.98 MA) exhibit a similar rise in pedestal pressure with density, reaching $p_{\text{ped}} \sim 30$ kPa (figure 4(a)). The measured pedestal pressure in figure 4 is determined by summing the electron pedestal pressure from a modified tanh fit to Thomson scattering data with ion pressure obtained via charge exchange measurements in a single channel near the pedestal top. The observed trajectory

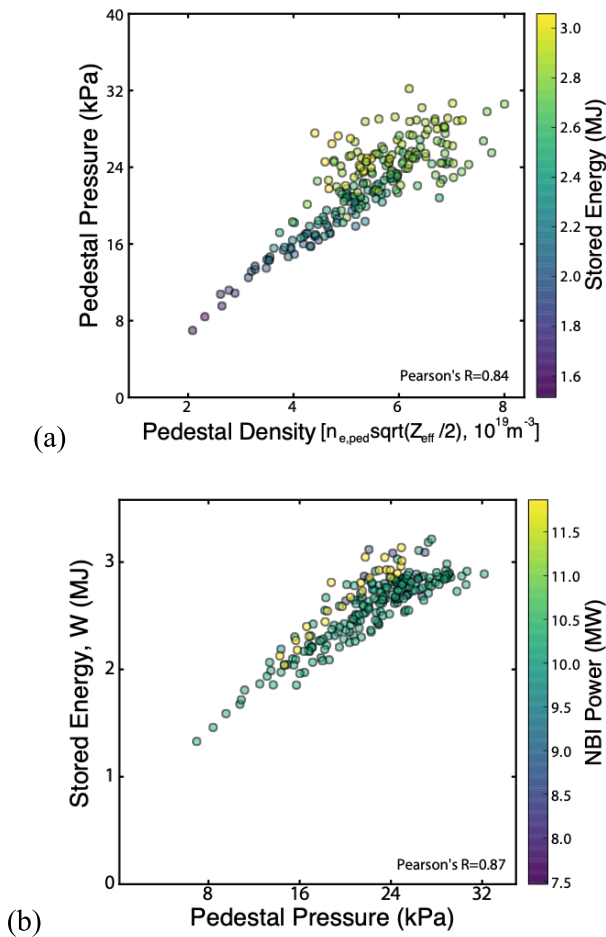


Figure 4. (a) Observed pedestal pressure versus pedestal density $[n_{e,ped} (Z_{eff}/2)^{1/2}]$ for DIII-D Super H experiments at $I_p = 1.8\text{--}1.98$ MA, during the initial rise ($t = 1800\text{--}2300$ ms). Stored energy, W_{MHD} , is indicated by the colorbar at right. (b) Stored energy, W_{MHD} , as a function of pedestal pressure, with neutral beam injected power indicated by the colorbar at right. In both parts of this figure, Pearson's correlation coefficient between the quantities on the two axes is given in small text on the body of the plot.

follows theoretical expectations (\sim linear increase in p_{ped} with $n_{e,ped}$) consistent with a rise into the NSH and SH regimes at higher density. As the pedestal pressure rises, these experiments reach large peak stored energy ($W_{MHD} \sim 2.4\text{--}3.2$ MJ), the highest values recorded in the present (with existing in-vessel pumps and limiters) configuration of DIII-D. These large values of W_{MHD} are obtained with modest injected power ($P_{nbi} \sim 8\text{--}12$ MW, no RF/EC power, negligible Ohmic power $< \sim 0.2$ MW) as shown in figure 4(b), roughly half the available power on DIII-D, consistent with high energy confinement ($\tau_E \sim 0.2\text{--}0.7$ s, $H_{98} \sim 1.6\text{--}2.5$) during this time.

The combination of high core ion temperature ($T_{i0} \sim 14\text{--}18$ keV), stored energy (2–3.2 MJ) and confinement are favorable for fusion performance, and these discharges exhibit significant DD fusion despite modest values of field ($B_t = 2.1\text{--}2.2$ T) and current ($I_p = 1.6\text{--}1.98$ MA), and the medium size of DIII-D ($a \sim 0.6$ m, $R \sim 1.67$ m, $V \sim 20$ m³). In the remainder of this section (figures 5 and 6) we consider cases with $T_{i0} > 12$ keV. Peak DD neutron rates as high as $1.86 \cdot 10^{16}/s$ are measured (figure 5(a)), via a plastic scintillator

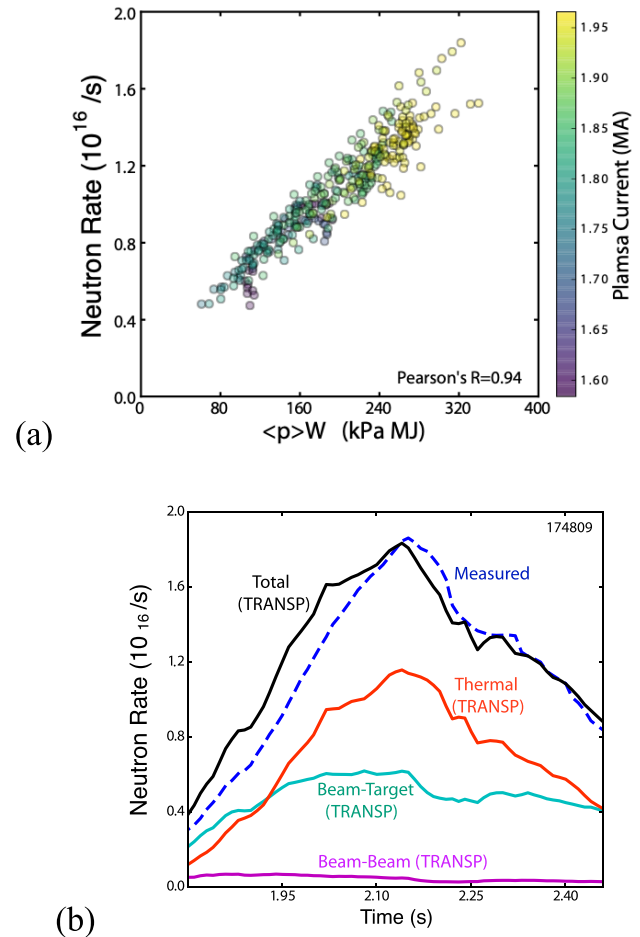


Figure 5. (a) Measured neutron rate versus the product of volume average pressure and stored energy, $\langle p \rangle W$. The plasma current (I_p) is given by the colorbar, and Pearson's correlation coefficient (0.94) between the quantities plotted on the two axes is given in small text. (b) TRANSP simulation of total neutron rate (black line) versus time, compared to measured value (dashed blue line) for DIII-D 174809. The thermal, beam-target, and beam-beam neutron rates from TRANSP are also indicated.

with $\sim 15\%$ uncertainty [25]. The roughly linear increase, and strong correlation ($r = 0.94$), in neutron rate with volume average pressure times stored energy, $\langle p \rangle W$, shown in figure 5(a), is consistent with predominantly thermal neutrons (a much weaker correlation, $r = 0.34$, is found to NBI power). Analysis with TRANSP [26] predicts total neutron rate (black line) consistent with measurements (blue dashed line), (provided a good match is obtained in W), and indicates that $\sim 2/3$ of the neutrons are produced by thermal reactions, while $\sim 1/3$ are beam-target and beam-beam reactions (with a small fraction from beam-beam), as shown in figure 5(b).

TRANSP has also been used to assess the equivalent DT fusion performance of these discharges. This is done by fixing a 0.4 ion fraction of tritium (and reducing the D fraction by an equivalent amount), while keeping the carbon impurity fraction unchanged. These simulations find an increase of a factor of ~ 222 in thermal fusion power going from DD to DT fuel, consistent with prior studies at similar T_i [24]. In a DD plasma, each neutron indicates a reaction in each branch, for a total energy of 7.3 MeV per neutron, and the measured

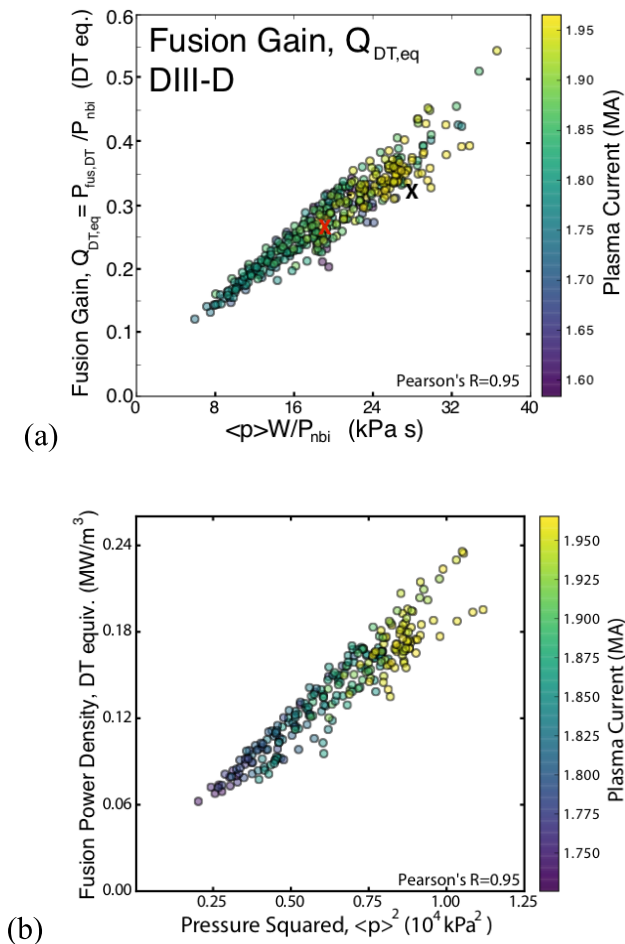


Figure 6. (a) DT equivalent fusion power gain, $Q_{DT,eq} = P_{fus,DT,eq}/P_{nbi}$ versus $\langle p \rangle W/P_{nbi}$. Shots from 2017–18 DIII-D Super H experiments are indicated by colored circles with color indicating plasma current. For comparison the previous highest Q shot from DIII-D (black X, shot 87977) [24] and a similar shot (red X, shot 87937) are shown. (b) DT equivalent fusion power density versus square of the volume average plasma pressure, $\langle p \rangle^2$. In both plots, Pearson's correlation coefficient is indicated in small text.

peak neutron rate of $1.86 \times 10^{16} \text{ s}^{-1}$ corresponds to a peak DD fusion power of 22 kW, and an equivalent DT power $\sim 222 \times$ this amount, or 4.8 MW. Because neutral beam power can vary with time (feedback control of β_N by varying beam power is employed in some discharges), a causal Gaussian back-average over twice the beam slowing time ($\tau_s \sim 40$ ms) is used in calculating the effective neutral beam heating power P_{nbi} . DT equivalent fusion gain ($Q_{DT,eq}$), the ratio of DT equivalent power to auxiliary power, has been defined in various ways in the literature. We first employ the simple definition used by [24], $Q_{DT,eq} = P_{fus,DT,eq}/P_{nbi}$. P_{nbi} is the neutral beam power, with causal Gaussian back average over $2\tau_s \sim 80$ ms (Ohmic power is small, <0.4 MW, and no other auxiliary power is used here, as in [24], and only cases where dW/dt is positive or nearly zero, $dW/dt > -0.2$ MW, are included). $Q_{DT,eq}$ is plotted as a function of $\langle p \rangle W/P_{nbi}$ in figure 6(a). Values as high as 0.54 are achieved in cases with time varying P_{nbi} , and values as high as 0.45 in cases where P_{nbi} is

constant across the high fusion power phase. For comparison, the prior highest peak $Q_{DT,eq}$ value (~ 0.32) from DIII-D 87977 is plotted (black X) in figure 6(a) (along with a similar shot, 87937, as the red X). Note that alternate definitions of Q have been employed in the literature. If P_{nbi} is replaced by $P_{loss} = P_{nbi} - dW/dt$, then a maximum value of $P_{fus,DT,eq}/P_{loss} \sim 1$ is found (in DIII-D 174791). If the definition used by JT-60U [27] is employed, where fusion power is divided into thermal ($P_{fus,DT,th}$) and beam-driven ($P_{fus,DT,b}$) components, with $Q_{DT,eq}^* = P_{fus,DT,b}/P_{nbi} + P_{fus,DT,th}/(P_{nbi} + P_{OH} - dW/dt - 0.2P_{fus,DT,th})$, the maximum value in the DIII-D SH/NSH dataset is $Q_{DT,eq}^* \sim 0.9$. The DT equivalent fusion power density is plotted versus the square of the volume average pressure in figure 6(b) for a subset of these cases, with $1.7 \text{ MA} < I_p < 2.0 \text{ MA}$. The maximum DT equivalent fusion power density shown ($\sim 0.23 \text{ MW m}^{-3}$) is similar to values reported on JT-60U [27] and JET [28], and to previously reported values on DIII-D [24]. Peak values of $\langle p \rangle_{\tau_E} \sim 65 \text{ kPa s}$, and $n_{i0}T_{i0}\tau_E \sim 7 \cdot 10^{20} \text{ m}^{-3} \text{ keV s}$ are achieved. Note that in the high $Q_{DT,eq} > 0.3$ DIII-D cases shown here, the high Q condition is maintained only briefly (~ 0.1 – 0.4 s), as is the case in prior high Q DIII-D cases [24] and reported high Q cases on other devices [27, 28]. The important issue of sustainment is discussed in the following section.

3. Sustainment and core-edge compatibility

High pedestal pressure and peak performance indicate the potential of the Super H and Near-Super H regimes as attractive regimes of operation for a fusion device. However, to fully realize this potential, it is necessary both to sustain high confinement and pressure, and to demonstrate consistent core-edge solutions including a high density near the separatrix, and strongly dissipative divertor.

An important challenge for sustainment of high confinement states is the control of density and impurity accumulation. On DIII-D, small $n = 3$ magnetic perturbations produced by internal coils ('I-coil') have enabled stationary density and pressure without impurity accumulation, enabling high performance ($\beta_N \sim 2.9$, $H_{98} \sim 1.6$, $\tau_E \sim 0.2$ s, $W \sim 1.9$ MJ) for the programmed duration of the shot. Figure 7 compares similar $I_p = 1.6$ MA DIII-D shots with (red) and without (black) an $n = 3$ perturbation applied from 2.3–4.4 s. By employing the $n = 3$ perturbation (and a target value of $\beta_N = 3$ in the NBI power feedback algorithm), uncontrolled density accumulation and onset of large core tearing modes are avoided, enabling sustained operation. While fusion performance is substantially reduced from the peak values discussed in the previous section (in part due to ion-electron equilibration and reduction of $T_{i,0}$ from maximum values of ~ 16 keV to stationary values ~ 8 keV) it remains high, with sustained values of $\langle p \rangle_{\tau_E} \sim 12 \text{ kPa s}$, $n_{i0}T_{i0}\tau_E \sim 0.9 \cdot 10^{20} \text{ m}^{-3} \text{ keV s}$, and $Q_{DT,eq} \sim 0.14$. The drop in confinement time from the peak values to the stationary state appears to primarily result from ion-electron equilibration and the resulting drop in T_i/T_e and the pedestal ion temperature, reduction of the global beta limit

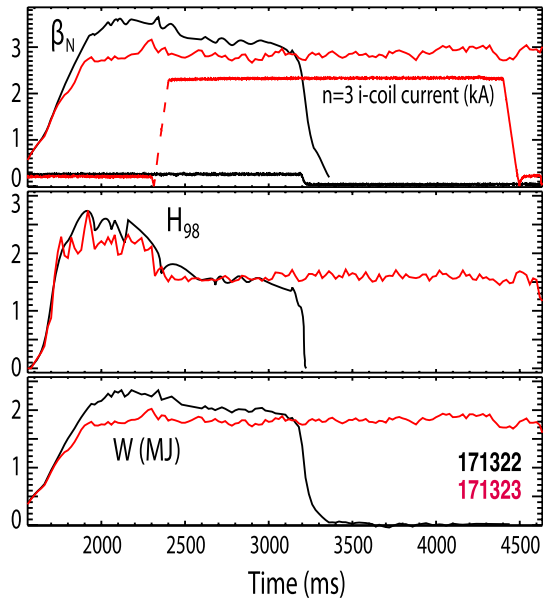


Figure 7. Time traces for discharges without (black) and with (red) a 2.5 kA $n = 3$ I-coil perturbation. The top figure shows β_N (top two traces), overlaid with $n = 3$ current from the I-coil. The middle figure shows normalized confinement ($H_{98,y2}$) and the bottom figure shows stored energy.

due to broader current profile, reduced rotation, and in some cases core tearing mode onset. Detailed study of core transport is in progress.

Because the pedestal in the SH and NSH regimes is predicted to be limited by current-driven kink-peeling modes (see e.g. red and blue lines in figures 1(b), 2(a) and (b)), the near-linear increase in predicted pedestal pressure with pedestal density indicates a pedestal limited by current-driven modes, it is expected that increasing the density near the separatrix will not negatively impact pedestal stability or pedestal pressure. This is in contrast to predictions and observations in cases where the pedestal is limited by pressure driven modes (see e.g. the rightmost black lines in figures 1(b), 2(a) and (b)), where the pedestal pressure is predicted to degrade with density (and can degrade even further if resistivity becomes sufficient to strongly drive resistive ballooning modes). This degradation of pedestal pressure with density can be particularly problematic in metal wall machines, which often use strong gas puffing to protect metal surfaces from erosion [6, 29]. Along the SH/NSH branch, it is predicted that solutions with both high pedestal pressure and high density, including high separatrix density, are realizable and may make attractive core-edge operational regimes.

To test this hypothesis, a scan of D_2 gas rate has been conducted in a series of DIII-D discharges with $I_p = 1.95$ MA, $B_t = 2.17$ T, $\delta \sim 0.6$, $q_{95} \sim 3.8$. Figure 8 compares cases with D_2 gas rates (lower traces in figure 8(a)) of 3, 50, 70 and 110 Torr $l\ s^{-1}$, applied from $t = 2.8$ –4 s. Applying these levels of gas puffing does not significantly impact either $\tau_E \sim 0.14$ s (figure 8(a), upper traces), or p_{ped} (figure 8(b)). The pedestal density in these cases is held approximately constant at $\sim 7 \times 10^{19} m^{-3}$ (figure 8(c), upper traces) by employing feedback control of

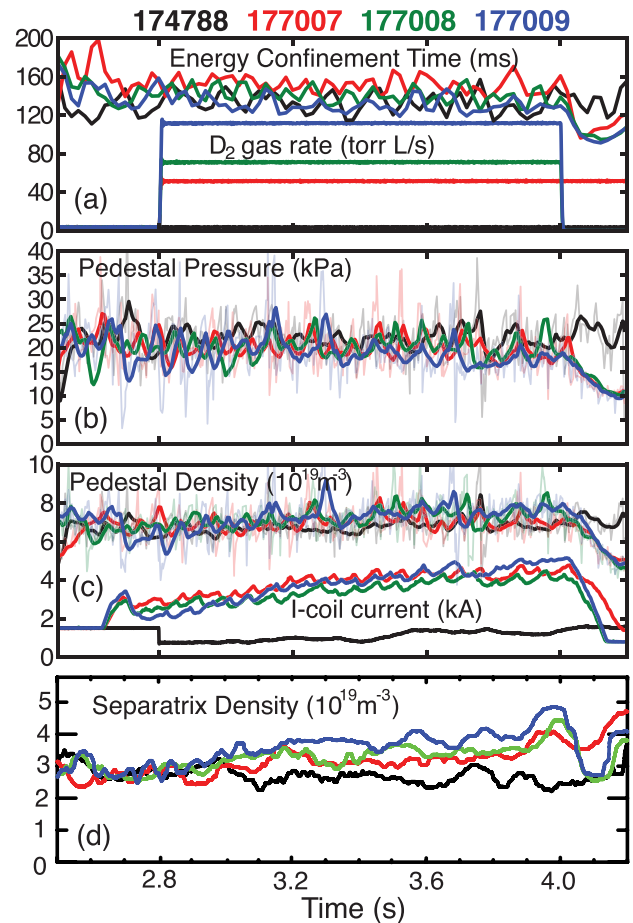


Figure 8. Time evolution of 4 DIII-D shots with varying D_2 gas rates and I-coil feedback control of pedestal density. (a) Energy confinement time (top fluctuating traces) and deuterium gas rate (lower flat traces), (b) pedestal pressure in kPa, (c) pedestal electron density (above) and $n = 3$ current from the I-coil (below), (d) electron density at the separatrix.

line average density by varying the i-coil current (figure 8(c), lower traces). However, the separatrix density (figure 8(d)) increases significantly from $\sim 2.5 \times 10^{19} m^{-3}$ to $\sim 4 \times 10^{19} m^{-3}$ as the gas rate is increased. Note that in the strong fueling case, both the pedestal and separatrix density are in the range of ITER design values [30], while no significant degradation of either core confinement or pedestal pressure is associated with increased gas puffing (note that all cases shown in figure 8 have large core tearing modes and somewhat reduced confinement relative to discharges without these modes such as 171323 in figure 7). The strike point T_e at the outer divertor plate is reduced by a factor of ~ 2 in the strong fueling case (from ~ 45 eV to ~ 22 eV), and the strike point density increases by a similar factor, reaching values $\sim 7 \times 10^{19} m^{-3}$.

Introducing a radiative impurity, such as N_2 , can further improve divertor performance. In DIII-D 177018, a combination of 37 Torr $l\ s^{-1}$ of D_2 gas, and feedback controlled N_2 injection (as in [31]), with a target of 5 MW of divertor radiated power, is used to enhance radiative losses in the divertor. This combination leads to substantial reduction of T_e , and enhancement of n_e , near the outer strike point, as shown in figure 9. The divertor radiated power reaches its target value

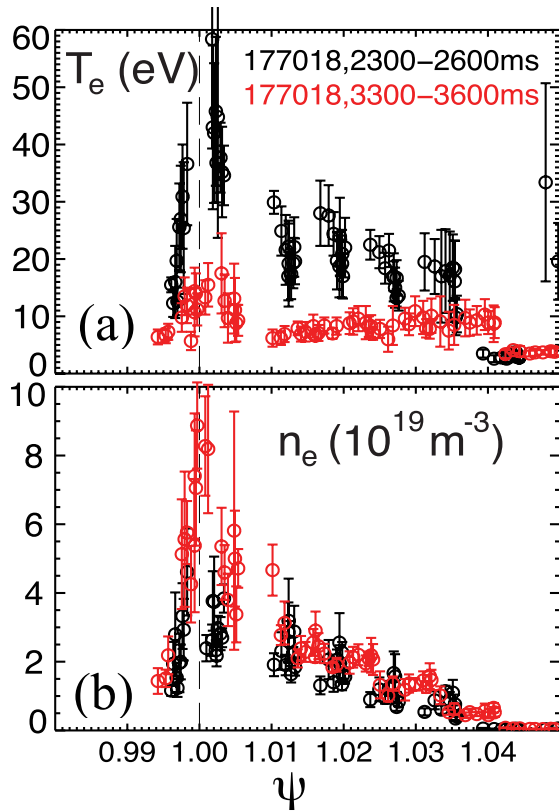


Figure 9. Measurements of outer divertor T_e (above) and n_e (below), before (black) and after (red) a combination of D_2 and N_2 fueling.

of ~ 5 MW, while total radiative losses are ~ 7.5 MW (out of a total injected power of 12 MW), with no appreciable degradation of pedestal pressure or confinement time. Much larger values of N_2 injection do lead to degradation as radiative losses become very large.

4. Simple metrics of fusion performance

In addition to C-Mod and DIII-D, SH/NSH operation is predicted to be possible at high density on ITER (figure 10(a)), as well as in strongly shaped discharges in JET and JT-60SA. A full assessment of predicted SH/NSH performance requires coupled core-pedestal simulation [11–14]. It is also useful to consider simpler performance metrics to compare regimes. The expression for fusion gain, $Q = P_{\text{fus}}/P_{\text{aux}}$, or similarly fusion power divided by total heating power (Q^+):

$$Q^+ = \frac{P_{\text{fus}}}{P_h} = \frac{P_{\text{fus}}}{P_{\text{aux}} + P_\alpha} = \frac{Q}{1 + Q/5} \quad (1)$$

for DT fusion, can be simplified by writing the fusion power in terms of a peaking, fusion reaction energy and T_i factor (f_p):

$$P_{\text{fus}} = f_p \langle p \rangle^2 V = \frac{2}{3} f_p \langle p \rangle W. \quad (2)$$

The total heating power (including auxiliary and charged fusion product power), $P_{\text{aux}} + P_\alpha$, can then be cast in terms of a multiplier (f_{LH}) of a simplified LH transition power scaling:

$$P_h = P_{\text{aux}} + P_\alpha = f_{\text{LH}} c_{\text{LH}} n_e B_t S \quad (3)$$

(where S is plasma surface area and c_{LH} is a nearly constant scale factor), or, replacing density (n_e) with Greenwald fraction,

$$P_h = P_{\text{aux}} + P_\alpha = f_{\text{LH}} c_{\text{LH}} f_{\text{GW}} B_t S I_p / \pi a^2. \quad (4)$$

Rewriting volume averaged pressure $\langle p \rangle$ in terms of a core peaking factor, $f_c = \langle p \rangle / p_{\text{ped}}$, and the Troyon normalized pedestal pressure $\beta_{\text{N,ped}}$, one finds:

$$Q^+ = f_q I_p a B_t \quad (5)$$

where f_q is an overall ‘quality factor’ which scales with $f_p f_c^2 \beta_{\text{N,ped}}^2 / f_{\text{GW}} f_{\text{LH}}$. For example, for ITER to achieve $Q = 10$ ($Q^+ = 10/3$), at $I_p = 15$ MA, $B_t = 5.3$ T, $a = 2$ m, requires a quality factor $f_q = 0.021$ (in units of $\text{T}^{-1} \text{MA}^{-1} \text{m}^{-1}$). DIII-D Super H experiments have achieved significantly higher values of DT equivalent f_q both peak (~ 0.21 , or ~ 0.14 with only thermal fusion) and sustained (~ 0.08 , or ~ 0.03 with only thermal fusion), with important caveats including that these discharges include strong co-torque (and strong co-rotation), have $T_i > T_e$, and do not suppress ELMs. Because Q^+ is highly sensitive to T_i (via the f_p factor), it is valuable to remove this dependence and consider the closely related metric, $Q^+ / (2/3 f_p) = \langle p \rangle W / P_h$. From above ($Q^+ = f_q I_p a B_t$), one can then define a modified quality factor:

$$f'_q = f_q / (2/3 f_p) = \langle p \rangle W / P_h I_p a B_t \quad (6)$$

which scales as $f_c^2 \beta_{\text{N,ped}}^2 / f_{\text{GW}} f_{\text{LH}}$, and enables comparisons of discharges with a wide range of T_i . This quality $f'_q = \langle p \rangle W / P_h I_p a B_t$ factor also has the convenient form of the ratio of a simple metric of fusion performance, $\langle p \rangle W$, divided by each of the key inputs (heating power, current, size and magnetic field) needed to achieve that performance. As shown in figure 10(b), Super H experiments on DIII-D and C-Mod have achieved large values of this factor, sufficient for high gain ($Q = 10$) on ITER at $I_p < 15$ MA. Operation below 15 MA is expected to both reduce the frequency and the impact of disruptions.

5. Discussion and future work

A set of experiments on Alcator C-Mod and DIII-D, guided by theoretical predictions of the Super H (and Near Super H) regime, have achieved high pedestal pressure and global fusion performance. Pedestal pressure up to ~ 80 kPa has been achieved on C-Mod at toroidal and poloidal field near the ITER value, extending tests of the EPED model nearly to the ITER predicted p_{ped} . High stored energy and peak fusion performance have been achieved on DIII-D, including DT equivalent fusion gain $Q_{\text{DT,eq}} \sim 0.5$ and $\langle p \rangle \tau_E \sim 65$ kPa s, at modest current (1.95 MA), field (2.17 T) and size ($a \sim 0.6$ m, $V \sim 20 \text{ m}^3$).

By employing $n = 3$ magnetic perturbations to control density and impurity accumulation, sustained operation at high

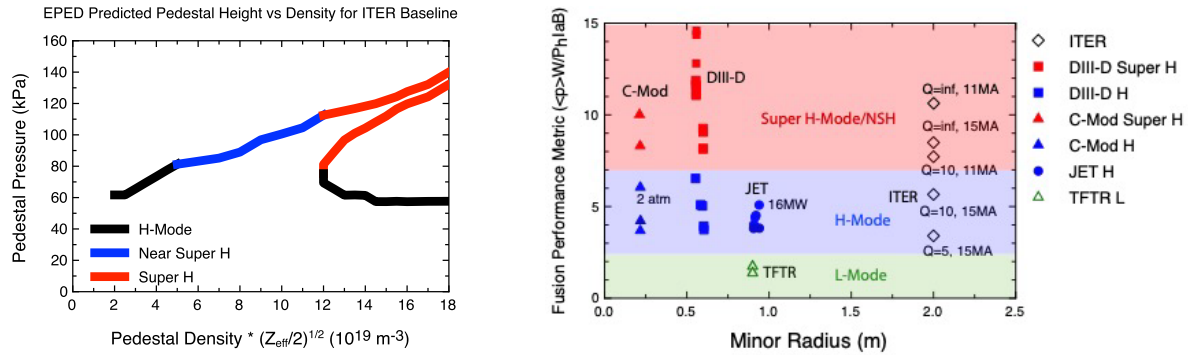


Figure 10. (a) EPED predictions of pedestal pressure in ITER baseline (15 MA), including the NSH (blue) and SH (red) regimes. (b) Fusion performance metric $\langle p \rangle W / P_h I_p a B_t$ (in kPa s/MA m T) shown for Super H experiments on C-Mod (red triangles) and DIII-D (red squares) compared to H-mode (blue) and L-mode (green) discharges on existing machines. Also shown are the approximate required values of this metric for various levels of performance on ITER (open diamonds).

performance ($\beta_N \sim 2.9$, $H_{98} \sim 1.6$, $\tau_E \sim 0.2$ s, $W \sim 1.9$ MJ) has been achieved on DIII-D for the full hardware-limited duration of the discharge (~ 2.5 s). Divertor temperature has been reduced, and divertor radiated power increased, via puffing of D_2 and N_2 gas, without significant degradation of p_{ped} or core confinement.

There are numerous important directions for future exploration of the SH and NSH regimes, including (a) ELM suppression in co-injected discharges, (b) compatibility with full divertor detachment, (c) compatibility of sustained discharges with low torque, (d) understanding of tearing mode onset, (e) resistive wall mode physics, (f) exploration of high-Z transport, and (g) larger bootstrap fraction. Addressing ELM suppression and mitigation is particularly important in regimes with high pedestal stored energy. The results presented here with metal wall and no injected torque (C-Mod) and with carbon wall and substantial neutral beam torque (DIII-D) suggest that access to the SH/NSH regime and very high pedestal pressure is not dependent on torque or wall material, however it is expected that sustainment in metal wall devices will be particularly dependent on maintaining cool, radiative divertor conditions. Extension of the Super H regime to devices beyond DIII-D and C-Mod is also of strong interest. The very high peak performance, potential for sustainment, and compatibility with high density separatrix and divertor, all suggest that the SH/NSH regimes hold promise for attaining elevated fusion performance on ITER and future devices. Control of ELMs, avoidance (or strong mitigation) of disruptions, and stationary operation at low torque are key challenges for developing this regime on ITER.

Finally, we note that achievement of high values for metrics such as $f_q = Q^+ / I_p a B_t$ and $f_q' = \langle p \rangle W / P_h I_p a B_t$, is a key element for enabling cost-effective, compact fusion devices at modest plasma current. Furthermore, the ability to predict access to very high pedestal regimes such as SH/NSH, and to predict coupled core-pedestal performance (as in [11–14]), potentially enables substantial improvement and optimization of future device designs. Initial theoretical studies and experimental results presented above, identify a promising regime at

strong shaping ($\delta > 0.45$, $\kappa \sim 1.6$ – 2.1), moderate aspect ratio ($R/a \sim 2.5$ – 3), and moderate $q_{95} \sim 3.5$ – 5 . The combination of strong magnetic field, facilitated by high temperature superconductors, and high sustained f_q in the SH/NSH regime should enable ignition and sustained fusion burn in devices that are modest in size with modest plasma current (which facilitates high bootstrap current fraction and low recirculating power, and also mitigates disruption concerns), significantly improving the attractiveness of a future fusion pilot plant or reactor.

Acknowledgments











This material is based upon work supported by the US Department of Energy, Office of Science, Office of Fusion Energy Sciences, under Awards DE-FC02-04ER54698, DE-FC02-99ER54512, DE-FG02-95ER54309, DE-FC02-06ER54873, DE-SC0014264, DE-AC02-09CH11466, and DE-SC0017992, using the DIII-D National Fusion Facility and Alcator C-Mod, DOE Office of Science user facilities. Extensive discussions with the ITPA pedestal group, as well as the numerous contributions of the Alcator C-Mod team, DIII-D team, and OMFIT group are gratefully acknowledged.

Disclaimer

This report was prepared as an account of work sponsored by an agency of the United States Government. Neither the United States Government nor any agency thereof, nor any of their employees, makes any warranty, express or implied, or assumes any legal liability or responsibility for the accuracy, completeness, or usefulness of any information, apparatus, product, or process disclosed, or represents that its use would not infringe privately owned rights. Reference herein to any specific commercial product, process, or service by trade name, trademark, manufacturer, or otherwise does not necessarily constitute or imply its endorsement, recommendation, or favoring by the United States Government or any agency thereof. The views and opinions of authors expressed herein

do not necessarily state or reflect those of the United States Government or any agency thereof.

ORCID iDs

P.B. Snyder  <https://orcid.org/0000-0002-0613-4232>
 J.W. Hughes  <https://orcid.org/0000-0003-4802-4944>
 C. Paz-Soldan  <https://orcid.org/0000-0001-5069-4934>
 M. Knolker  <https://orcid.org/0000-0002-8468-8767>
 D. Eldon  <https://orcid.org/0000-0003-1895-0648>
 T. Evans  <https://orcid.org/0000-0002-8357-5859>
 B.A. Grierson  <https://orcid.org/0000-0001-5918-6506>
 B. LaBombard  <https://orcid.org/0000-0002-7841-9261>
 F.M. Laggner  <https://orcid.org/0000-0003-1601-2973>
 H.R. Wilson  <https://orcid.org/0000-0003-3333-7470>

References

- [1] Snyder P.B. et al 2011 *Nucl. Fusion* **51** 103016
- [2] Snyder P.B. et al 2012 *Phys. Plasmas* **19** 056115
- [3] Snyder P.B. et al 2009 *Phys. Plasmas* **16** 056118
- [4] Snyder P.B. et al 2009 *Nucl. Fusion* **49** 085035
- [5] Beurskens M. et al 2011 *Phys. Plasmas* **18** 056120
- [6] Leyland M. et al 2015 *Nucl. Fusion* **55** 013019
- [7] Walk J.R. et al 2012 *Nucl. Fusion* **52** 063011
- [8] Hughes J.W. et al 2013 *Nucl. Fusion* **53** 043016
- [9] Groebner R.J. et al 2013 *Nucl. Fusion* **53** 093024
- [10] Komm M. et al 2017 *Nucl. Fusion* **57** 056041
- [11] Meneghini O. et al 2016 *Phys. Plasmas* **23** 042507
- [12] Meneghini O. et al 2018 Neural-network accelerated coupled core-pedestal simulations with self-consistent transport of impurities *Preprint: 2018 IAEA Fusion Energy Conf. (Gandhinagar, India, 22–27 October 2018)* TH/P6-16
- [13] Park J.M. et al 2018 Integrated modeling of core, edge pedestal and scrape-off-layer for high β_N steady-state scenarios on DIII-D *Preprint: 2018 IAEA Fusion Energy Conf. (Gandhinagar, India, 22–27 October 2018)* TH/P7-2
- [14] Buttery R.J. et al 2018 The advanced tokamak path to a compact net electric fusion pilot plant *Preprint: 2018 IAEA Fusion Energy Conf. (Gandhinagar, India, 22–27 October 2018)* FIP/P3-26
- [15] Solomon W. et al 2014 *Phys. Rev. Lett.* **113** 135001
- [16] Snyder P.B. et al 2015 *Nucl. Fusion* **55** 083026
- [17] Garofalo A. et al 2015 *Phys. Plasmas* **22** 056116
- [18] Solomon W. et al 2016 *Phys. Plasmas* **23** 056105
- [19] Hughes J.W. et al 2011 *Nucl. Fusion* **51** 083007
- [20] Ma Y. et al 2012 *Nucl. Fusion* **52** 023010
- [21] Whyte D.G. et al 2010 *Nucl. Fusion* **50** 105005
- [22] Hubbard A.E. et al 2017 *Nucl. Fusion* **57** 126039
- [23] Hughes J.W. et al 2018 *Nucl. Fusion* **58** 112003
- [24] Lazarus E.A. et al 1997 *Nucl. Fusion* **37** 7
- [25] Heidbrink W.W. 1997 *Rev. Sci. Instrum.* **68** 536
- [26] Budny R.V. 1994 *Nucl. Fusion* **34** 1247
- [27] Ishida S. et al 1999 *Nucl. Fusion* **39** 1211
- [28] Keilhacker M. et al 2001 *Nucl. Fusion* **41** 1925
- [29] Dunne M.G. et al 2017 *Plasma Phys. Control Fusion* **59** 014017
- [30] Kukushkin A.S. et al 2009 *Nucl. Fusion* **49** 075008
- [31] Eldon D. et al 2019 Advances in radiated power control at DIII-D *Nucl. Mater. Energy* **18** 285